

Dynamic, self-assembled aggregates of magnetized, millimeter-sized objects rotating at the liquid-air interface: Macroscopic, two-dimensional classical artificial atoms and molecules

Bartosz A. Grzybowski,¹ Xingyu Jiang,¹ Howard A. Stone,² and George M. Whitesides^{1,*}

¹*Department of Chemistry and Chemical Biology, Harvard University, 12 Oxford Street, Cambridge, Massachusetts 02138*

²*Division of Engineering and Applied Sciences, Harvard University, Pierce Hall, Cambridge, Massachusetts 02138*

(Received 3 October 2000; published 21 June 2001)

This paper describes self-assembly of millimeter-sized, magnetized disks floating on a liquid-air interface, and rotating under the influence of a rotating external magnetic field. Spinning of the disks results in hydrodynamic repulsion between them, while the rotating magnetic field produces an average confining potential acting on all disks. The interplay between hydrodynamic and magnetic interactions leads to the formation of patterns. Theoretical analysis of hydrodynamic and magnetic forces indicates that the interactions in this system are similar to those acting in systems of finite numbers of particles behaving classically (“classical artificial atoms”). Macroscopic artificial atoms and molecules are described, and the rules governing their morphologies outlined.

DOI: 10.1103/PhysRevE.64.011603

PACS number(s): 82.65.+r, 87.15.Nn

INTRODUCTION

The formation of patterns by self-assembly has implications for chemistry [1,2], physics [3–5], materials science [6–19], and biology [10–12]. Although most research in self-assembly and self-organization has focused on static structures, dynamic systems [13–15]—those that develop order only when dissipating energy—are particularly interesting for their relevance to issues of complexity [16] and emergence [17]. In this work, we describe a dynamic, self-assembling system composed of a finite number (<40) of millimeter-sized, magnetized disks floating on a liquid-air interface, and subject to an external magnetic field produced by a rotating permanent magnet with a dipole length much longer (~6 cm) than the radii of the disks. In the presence of the rotating external field, the disks spin around their axes with angular frequency equal to that of the magnet [$\omega \sim 200\text{--}1200$ rpm (revolutions per minute)]. All disks are attracted towards the axis of rotation of the magnet, and are repelled by one another by a hydrodynamic repulsion associated with the motion of a fluid around a spinning disk. The interplay between attractive and repulsive interactions leads to formation of macroscopic patterns that are similar to those observed in *classical artificial atoms* [18], i.e., microscopic systems composed of finite numbers of interacting classical particles confined by an external field and repelling one another.

Classical artificial atoms (CAA) are interesting both theoretically and experimentally and have been the object of research for many decades. More than a hundred years ago, Mayer [19] studied the organization of permanent magnets floating on the surface of a liquid and subject to a central magnetic field. The multiring structures observed in Mayer’s experiments had many analogies with what was then thought

to be the structure of an atom. In fact, it was Mayer’s experiments that inspired Thompson to construct a classical model [18] that would explain the subatomic structure. Although this picture of classical atoms was inaccurate and has not been explored further in considering conceptual models of atoms, Thomson-type models are adequate for describing many systems composed of finite numbers of interacting particles that behave classically. In three dimensions, examples of such systems are ions in ion traps (Paul trap [20], Penning trap [21]), heavy ions in storage rings [22], and electrons trapped in bubbles above liquid helium [23]. In two dimensions, they include two-dimensional (2D) colloidal crystals [24] and electrons in quantum dots [25]. The organization of classical particles in two-dimensional systems has been extensively studied theoretically for different interparticle potentials and for various profiles of the confining external field [26–28].

In previous work [29], we studied a pattern-forming system of magnetic disks, all of which have the same size. The patterns we observed qualitatively reproduced those predicted theoretically for two-dimensional CAA’s [26–28]. Here, we show that this similarity in ordering reflects similar forms of interactions in both systems—our experimental system can thus be regarded as a macroscopic 2D classical artificial atom, in which the spinning disks are the constituent “particles.” We quantify both the hydrodynamic repulsive force between the disks and the central magnetic force acting on all disks. The equations we derive give the scaling properties of the forces acting in the system. We also extend our previous experimental findings and describe systems of millimeter-sized disks of *different* sizes that give rise to complex planar aggregates. Specifically, we investigate two types of aggregates: (i) those in which *one* disk is much larger than the others and (ii) those in which *two* disks are larger than the rest. In the first type of aggregates, the large disk organizes small disks into concentric shells processing around it; by pictographic analogy, we call the large disk “a nucleus,” the small disks “electrons,” and the aggregate an “artificial

*Author to whom correspondence should be addressed. Email address: gmwhitesides@gmwhgroup.harvard.edu

atom.” In aggregates with two large disks, the geometries of the structures are reminiscent of those of diatomic molecules, accordingly, we call these structures “artificial molecules.”

This paper is organized in three sections. In Sec. I we describe the fabrication of magnetized disks and the experimental setup. In Sec. II, we explain the theory of hydrodynamic and magnetic forces acting on the spinning objects. In Sec. III we describe the morphologies of the mixed-size aggregates and the rules governing the arrangement of pieces in these aggregates.

I. EXPERIMENT

The circular disks were fabricated by a two-step procedure. First, hollow polyethylene tubing (~ 1 mm ID (inner diameter), ~ 2 mm OD (outer diameter), Intramedic) was filled with poly (dimethylsiloxane) (PDMS, Dow Corning) doped with magnetite ($\sim 5\%$ to $\sim 30\%$ by weight), and the polymer was allowed to cure at 60°C for 2 h. The resulting composite was cut into slices ~ 400 μm thick using a custom-made precision cutter. The disks were placed at an ethylene glycol: water (3:1 by volume)/air interface, so that they were fully immersed in the liquid except for their top surface. Although the disks were slightly more dense than the liquid, they were maintained at the interface by capillarity. A permanent bar magnet (KIKA Labor Technik) of dimensions $L \sim 5.6$ cm \times $W \sim 4$ cm \times $T \sim 1$ cm was placed at a distance H (~ 2 – 4 cm) below the interface and rotated with angular velocity ω [Fig. 1(a)]. The magnet was magnetized along its longest dimension and had magnetization $M \sim 1000$ G/cm³. The images of the aggregates were taken with a CCD camera interfaced to a VHS recorder and were subsequently digitized using SCIONIMAGE software.

II. THEORY

A. Hydrodynamic repulsion

The magnetic moments of the disks floating at the liquid-air interface interact with the magnetic moment of the permanent magnet placed below the interface. When the magnet is rotated at angular velocity ω , the disks spin around their axes at the same angular velocity. The fluid motion associated with spinning results in a repulsive hydrodynamic interaction between the disks.

To model this interaction we consider the simplest aggregate composed of two rigid spheres of radius a spinning with angular velocity ω under the influence of magnetic torque τ , and fully immersed in a fluid of viscosity μ , uniform density ρ , and kinematic viscosity $\nu = \mu/\rho$. The model of two spinning spheres is simpler mathematically than that of two spinning disks and the differences should not be expected to affect the conclusions materially; the lack of explicitness in accounting for the free upper surface of the spinning objects should also not limit the conclusions [30]. We define a Reynolds number associated with a spinning sphere as $\text{Re} = \omega a^2/\nu$. For the sizes of objects used in our experiments ($a \sim 0.5$ – 1.2 mm), and for the rotational speeds ($\omega \sim 200$ – 1200 rpm), we estimate Re to be on the order of one. Although this value of Re is in a difficult range of Reynolds

numbers for which to do detailed analytical calculations, there is rationale for predicting trends using ideas from low(not zero)-Reynold’s-number hydrodynamics.

A single isolated sphere spinning with a low Reynolds number creates a velocity field $\vec{u}(\vec{r}) = a^3 \vec{\omega} \times \vec{r}/r^3$, where \vec{r} is the position vector measured from the sphere’s center [Fig. 1(b)]. The corresponding viscous torque is $\vec{\tau} = 8\pi\mu a^3 \vec{\omega}$. Let the two spheres have positions \vec{x}_1 and \vec{x}_2 , where the subscript distinguishes qualities referring to the two spheres. We assume that the separation $d = |\vec{x}_1 - \vec{x}_2| \gg a$, in which case each (neutrally buoyant) sphere translates with speed $O(a^3\omega/d^2)$, or velocity $\vec{V}_2 = a^3 \vec{\omega} \times (\vec{x}_2 - \vec{x}_1)/d^3$, due to the flow from the adjacent sphere ($\vec{V}_2 = -\vec{V}_1$) [31]. One sphere now moves in the flow created by the other sphere. If we work with disturbance variables (\vec{u}, \vec{p}) defined as

$$\vec{u}^\infty = \lim_{r \rightarrow \infty} \vec{u}(\vec{r}) \quad \text{and} \quad \vec{u}(\vec{r}) = \vec{u}(\vec{r}) - \vec{u}^\infty, \quad \vec{p}(\vec{r}) = p(\vec{r}) - p^\infty \quad (1)$$

(\vec{u}^∞ is the relative flow in the neighborhood of one sphere produced by the second sphere), then the steady velocity field relative to the particle satisfies the Navier-Stokes equation in the form given by

$$\mu \nabla^2 \vec{u} - \nabla \vec{p} = \rho (\vec{u}^\infty \cdot \nabla \vec{u} + \vec{u} \cdot \nabla \vec{u}^\infty + \vec{u} \cdot \nabla \vec{u}). \quad (2)$$

Scaling all velocities by ωa , and lengths by a , and noting that $\vec{u}^\infty = O[\omega a(a^3/d^3)]$, with the leading term corresponding to a linear flow, we obtain the dimensionless form of Eq. (2),

$$\nabla^2 \vec{u} - \nabla \vec{p} = \text{Re} [\varepsilon (\vec{u}^\infty \cdot \nabla \vec{u} + \vec{u} \cdot \nabla \vec{u}^\infty) + \vec{u} \cdot \nabla \vec{u}], \quad (3)$$

where $\text{Re} = \omega a^2/\nu$ and $\varepsilon = (a/d)^3 \gg 1$.

It is not possible to explain the origin of the hydrodynamic repulsion between the spinning spheres without including inertia [i.e., the terms multiplied by Re in Eq. (3)]. To simplify the scaling analysis (a detailed calculation requires the use of singular perturbation methods), we consider only the leading order flow, that is the flow produced by an applied torque, $\vec{u}_0(\vec{r}) = \vec{\omega} \times \vec{r}/r^3$, and to make analytical arguments we assume $\text{Re} < 1$. Because of the linear variation of the disturbance flow, the influence of inertia becomes significant at a dimensionless distance $(\varepsilon \text{Re})^{-1/2}$, where viscous terms balance the inertial terms in Eq. (3). Since $u_0 = O(r^{-2})$, the weak, torque-induced flow in this far field is $O(\varepsilon \text{Re})$, and this flow is thus responsible for an inertially generated force acting on a sphere,

$$F_h = O[\mu(\omega a)a\varepsilon \text{Re}] = O(\rho\omega^2 a^7/d^3). \quad (4)$$

The details of such a calculation can, in principle, follow the methodology outlined by Schonberg and Hinch for the lift force on neutrally buoyant particles in channel flows [32].

We should note that it is possible to think about the flow created by spinning spheres, by considering the lift force on an object in a shear flow of an inviscid fluid. This problem was treated by Authon [33], who obtained the hydrodynamic

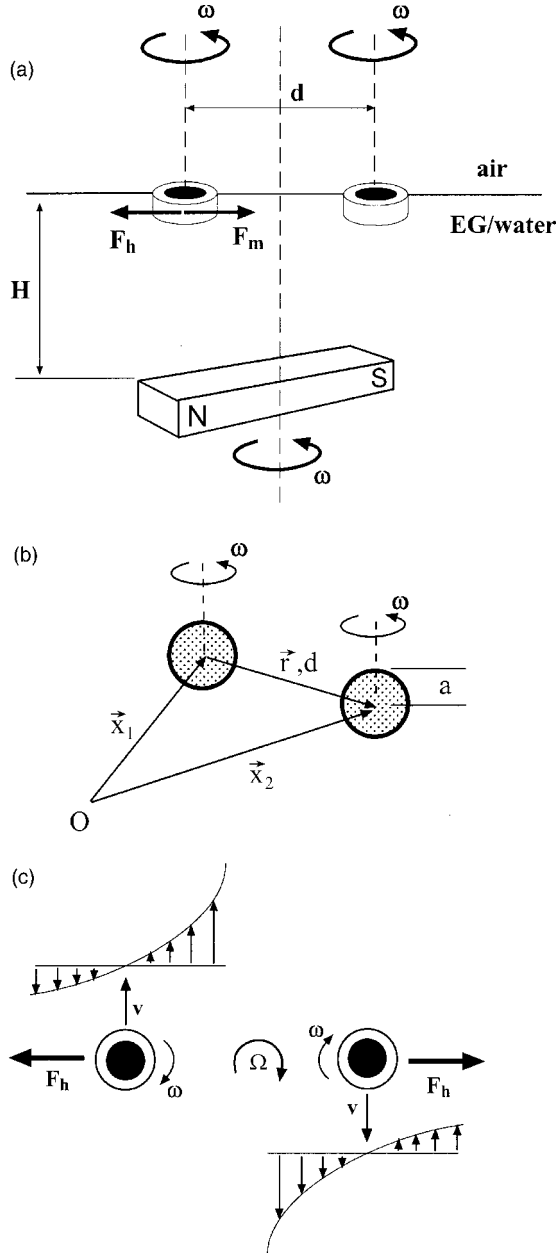


FIG. 1. (a) Schematic experimental setup. A rectangular magnet rotates at angular velocity ω (~ 200 – 1200 rpm) below a dish filled with liquid [a mixture of ethylene glycol (EG) and water]. The distance between the upper face of the magnet and the liquid-air interface is $H \sim 10$ mm. Magnetically doped disks (~ 1 mm in diameter) are placed on the interface and are immersed in the liquid except for their top surface. The disks spin at angular velocity ω around their axes and the entire aggregate slowly ($\Omega < 2$ rpm) precesses around its center. A magnetic force F_m attracts the disks towards the center of the dish and a hydrodynamic force F_h pushes them apart from each other. The picture in (b) defines the quantities used in calculations of the repulsive hydrodynamic force for two rotating spheres. (c) The scheme illustrates the origin of the repulsive hydrodynamic force for the simplest aggregate composed of two spinning disks. Each disk rotates, while simultaneously translating through a velocity gradient produced by the other disk; as a result, each disk experiences a lift force directed away from its neighbor.

lift force on a rigid sphere $\vec{F}_L = c_L \rho V \vec{U} \times \vec{\omega}^\infty$, where \vec{U} is the slip velocity of the sphere relative to the fluid and $\vec{\omega}^\infty = \vec{\Delta} \times \vec{u}_0$ is the vorticity of the flow evaluated at the location of the particle. In our system, in the frame of reference of the particle, the vorticity far away from the spinning sphere is $\vec{\nabla} \times \vec{u}_0 = (a/d)^3 (3\vec{\omega} \cdot \hat{d}\hat{d} - \vec{\omega})$, where \hat{d} is the unit vector along the line joining the centers of the spheres and $\vec{U}_0 = -(a^3/d^2)(\vec{\omega} \times \hat{d})$. Hence,

$$F_L \propto \vec{U}_0 \times \vec{\omega} = (a^6/d^5)(\vec{\omega} \times \hat{d}) \times (\vec{\omega} - 3d\vec{\omega} \cdot \hat{d}\hat{d}) \quad (5)$$

is directed away from the particle, and has magnitude $O(a^6 \omega^2/d^5)$. Balancing this force against the magnetic force $O(a^3)$ yields $\omega \propto d^{5/2}$ and $a \propto d^{5/3}$, which is not in good agreement with the data. This discrepancy is, however, not surprising since Auton in his analysis assumes $\omega a \ll |\vec{U}|$, which here requires $d^2/a^2 \ll 1$, which is clearly violated in our system.

B. Magnetic attraction

All disks are attracted towards the axis of rotation of the magnet by a centrosymmetric magnetic force. Consider a stationary, rectangular permanent magnet in a Cartesian frame of reference (Fig. 2), in which the x axis is along the longest dimension L of the magnet, and the z axis coincides with the axis of rotation of the magnet; the magnet has the magnetization vector M along the x axis. To calculate the magnetic induction produced by the magnet, we use a standard current-sheet method [34]. The magnet is divided into slices of thickness dx ; each slice produces a magnetic field equivalent to that of a current $i = Mc dx$ flowing in a loop enclosing the slice (shaded region in Fig. 2; c stands for the velocity of light). Integration over all slices gives the total field $\vec{B}(x, y, z)$ at location (x, y, z) ,

$$\vec{B}(x, y, z) = M \int_{-L/2}^{L/2} \oint_{\text{loop}} \frac{d\vec{l} \times \hat{s}}{s^2} dx, \quad (6)$$

where s is the distance between point (x, y, z) and a point on the path of integration. The integral over the loop can be evaluated analytically, but the integration along the x direction has to be carried out numerically. A ferromagnetic point object located at (x, y, z) experiences a magnetic force that has vector components proportional to the gradient of magnetic induction at this point. We approximated a disk by such a pointlike ferromagnetic object and calculated the gradient of the magnetic induction in the radial direction r (pointing from the axis of rotation of the magnet towards the disk) at the level of the liquid-air interface, $\partial B_r(x, y, H)/\partial r$, where B_r is the radial component of \vec{B} . Because, as we verified experimentally, the position of a disk does not change substantially during one revolution of the magnet ($\Omega \ll \omega$), the average, radially directed magnetic force acting on a disk can be calculated as the time average of $\partial B_r(x, y, H)/\partial r$ over one revolution of the magnet,

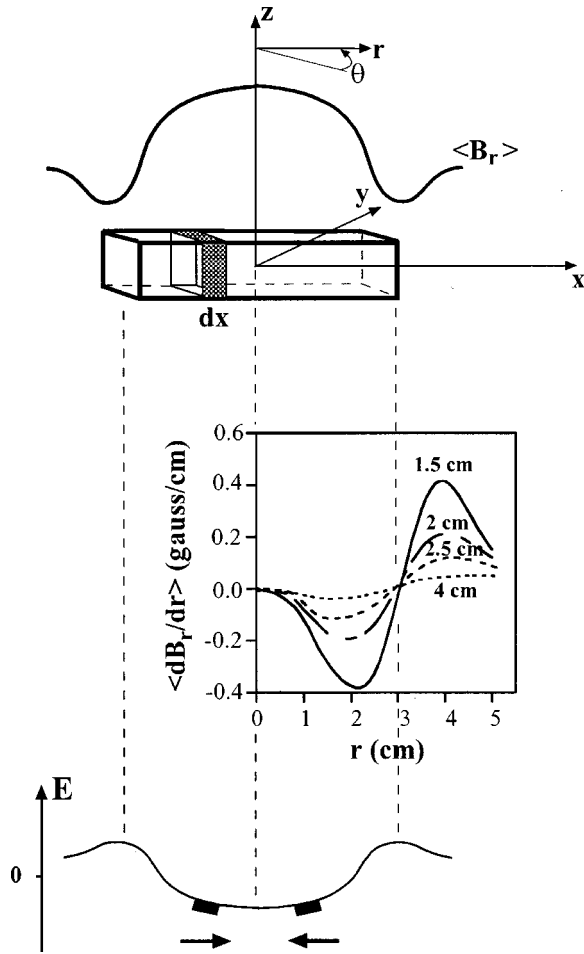


FIG. 2. The upper picture shows the system of coordinates used in the current-sheet calculations of the magnetic field. A qualitative profile of the radial component of magnetic induction $\langle B_r \rangle$ is also shown. The middle graph gives the profiles of the magnetic force F_m acting on a pointlike, ferromagnetic object floating at a liquid-air interface; the distances between the top face of the magnet and the level of the interface are indicated next to the curves. The bottom graph is a qualitative energy profile for ferromagnetic objects located at the liquid-air interface and subject to a magnetic field produced by a rotating permanent magnet.

$$F_m \propto \langle \partial B_r(x, y, H) / \partial r \rangle = \int_0^{2\pi} [\partial B_r(x, y, H, \theta) / \partial r] d\theta. \quad (7)$$

The dependence of the magnetic force on the radial position r is shown in the bottom graph in Fig. 2. The magnetic force is attractive (directed towards the center of the dish) within the circle of radius $r \sim L/2$; above this value, the magnetic force is repulsive. For the locations of the interface close to the upper face of the magnet ($H < \sim 2$ cm), F_m is a strongly varying function of r , and becomes slowly varying at $H \sim 4$ cm. We note that stable aggregates were formed only when $H > \sim 3$ cm; when the interface was too close to the magnet, the disks slowly orbited around the dish and no stable aggregates were observed.

C. Balance of forces and comparison with experiment

An aggregate assumes a stable configuration when the forces acting on the spinning disks balance. In our experiments, the distance between the upper face of the rotating magnet and the liquid-air interface is ~ 3 – 4 cm, so that the magnetic force F_m is only a slowly varying function of r (cf. Fig. 2). Also, for aggregates small compared to the longest dimension of the magnet L (e.g., a pair of disks), it is reasonable to assume that the magnetic field is roughly constant over the extent of the aggregate. With this assumption, the balance of forces for a pair of spheres (since the hydrodynamic estimates were performed for spheres, not disks) of the same radius can be written as in Eq. (8). The left-hand side of this equation represents the hydrodynamic repulsive force F_h acting on a sphere of radius a , and the right-hand side gives the magnetic force acting on a pointlike ferromagnetic object ($F_m \approx \text{const}$) [35] times the volume of the sphere ($V = 4/3\pi a^3$). This analysis then predicts that the separation d between the disks should depend on other parameters characterizing the system as

$$\rho \omega^2 a^7 / d^3 = \text{const} \times a^3, \quad (8)$$

$$d = \text{const}_2 \times \rho^{1/3} \omega^{2/3} a^{4/3}. \quad (9)$$

The constants in Eqs. (8) and (9) involve a function of H .

To verify the scaling predictions, we performed a series of experiments in which we related the center-to-center separation between the disks d to their angular velocity ω , disk radius a , solvent viscosity, and the strength of the confining magnetic field. The results of these experiments with rotating disks are in agreement with theoretical predictions for two rotating spheres, and are summarized in Fig. 3.

Figure 3(a) shows how the separation d varies with the rotational speed ω for disks of the same size (1.27 mm). The separation increases monotonically with ω . When plotted on a double-logarithmic plot (as in the inset to the figure), the slopes of the linear fits to the data are between 0.58 and 0.64, which is compatible with the theoretical prediction $d \sim \omega^{2/3}$. Further observations, detailed later, of many disks demonstrate that the separation between the nearest-neighbor disks is independent of the number of disks constituting the aggregate, suggesting that the interaction between the disks in large aggregates can be approximated as pairwise. Also, d is independent of the disk thickness (we confirmed this independence for disks of thicknesses 0.3–0.7 mm; disks thicker than 0.7 mm tend to wobble and the aggregates become unstable).

The dependence of d on disk sizes is shown in Fig. 3(b). For disks of different diameters (given in millimeters in the legend to the figure) and for a given ω , the separation between two disks increases with the sum of their diameters. For any pair of disks (of equal or different diameters), the separation between them increases with increasing ω (up to $\omega \sim 1000$ rpm). Our theoretical analysis predicts that for a pair of disks of equal sizes, and at a given ω , the distance between the disks should scale as $a^{4/3}$. Therefore, for two pairs of disks of equal sizes (a_1 in one pair, a_2 in the other), the ratio of separations between the disks in each pair,

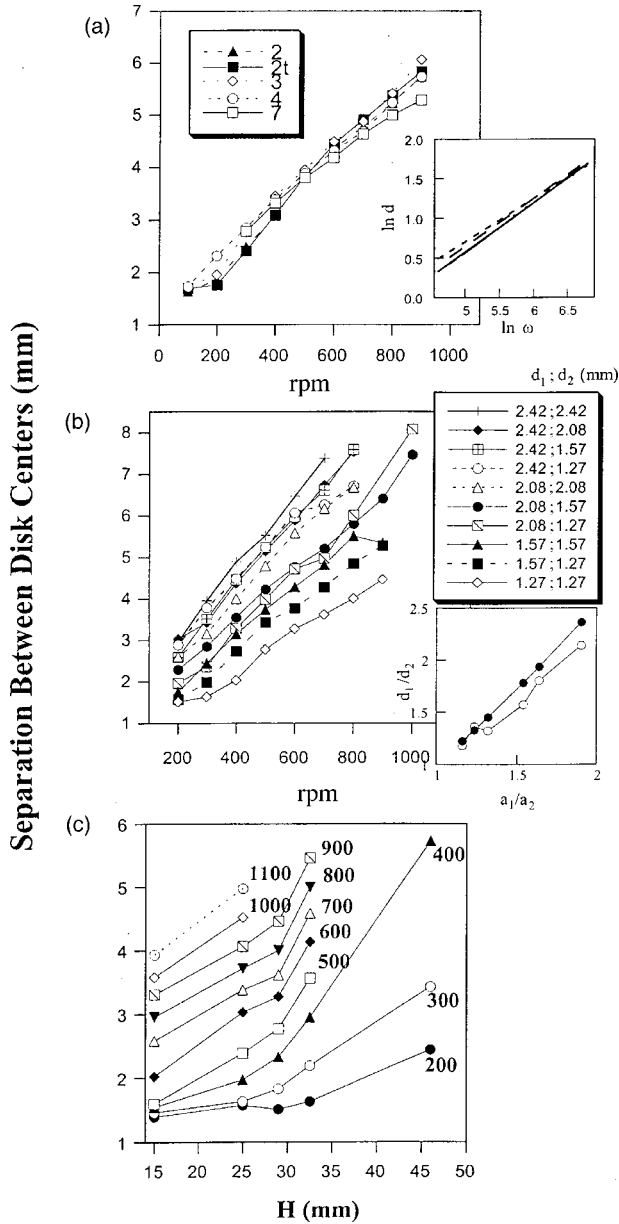


FIG. 3. The graphs give the separation between the centers of rotating disks as a function of ω and H . (a) For aggregates composed of different numbers of 1.27-mm disks (numbers of disks in the aggregates are given in the legend), the separation between nearest-neighbor disks increases with ω and does not depend on the number of disks composing an aggregate. For a given ω , the separation is independent of the disk thickness (for data labeled “2r” the thickness of the disks was 1 mm, in the other curves it was 0.5 mm). The inset is a double-logarithmic plot ($\ln \omega$ vs $\ln d$); the slopes of the lines in this plot are between 0.58 and 0.64, in good agreement with the theoretical prediction of $\frac{2}{3}$. (b) This figure shows how the separation between two disks of different sizes (given in the legend in millimeters) depends on the sizes of the disks. The inset illustrates how the separation between the disks of the same size scales with the disk radius (see text for details). The graph in (c) gives the spacing between two 1.27-mm disks for various distances between the interface and the top face of the magnet, H . Each curve corresponds to a different value of ω . The error bars for these data are smaller than the marker sizes.

d_1/d_2 , should scale as $(a_1/a_2)^{4/3}$. To test this prediction, we analyzed a set of four curves from Fig. 3(b) describing interactions between disks of equal sizes (i.e., 1.27 mm-1.27 mm, 1.57 mm-1.57 mm, 2.08 mm-2.08 mm, 2.42 mm-2.42 mm). In the inset to the figure, the ratios of disk sizes (a_1/a_2 , six possible combinations) vs the average value of the ratios of measured separations d_1/d_2 (open markers) is shown. We also plotted the values of d_1/d_2 expected from the theoretical analysis (solid markers). The experimental data are in good agreement with the theoretical expectation.

The solvent properties do not have a significant effect on hydrodynamic interactions in the system. For example, Eq. (9) predicts that the separation between the spinning objects should be independent of the viscosity of the liquid. We found that at a given ω , d is independent of the viscosity of the liquid over the range of kinematic viscosities $\nu \sim 1-50$ cP (the stability of *aggregates*, however, depends on viscosity; most stable structures were observed for $\nu > \sim 3$ cP). Since the hydrodynamic repulsion is inertial in character, the theory also predicts that d should show a weak dependence on the density of the fluid. For the relatively narrow range of densities used in our experiments ($\rho \approx 1.0-1.1$ g/cm³), the changes in d due to changes in density were too small to be quantified.

Figure 3(c) illustrates the effect of varying the magnitude of the confining magnetic field on the interdisk separation. As the distance between the upper face of the magnet and the level of the interface H increases, the magnitude of the magnetic field acting on the floating objects decreases, while the hydrodynamic interaction remains unchanged. Consequently, for a given ω , the separation between the disks increases with H .

D. Comparison of the potentials for spinning disks and for classical artificial atoms

The confining external potentials used in models of classical atoms are usually either parabolic [$V_C(r) \propto r^2$] or hard wall [$V_C(r) = 0$ if $r < R_C$ and $V_C(r) = \infty$ if $r > R_C$] [26,27]. In our system, for $H \sim 3-4$ cm, the slowly varying magnetic force can be approximated by piecewise linear functions of r , i.e., $F_m = -c'_1 r$ if $r < L/4$ and $F_m = c'_1 (r - L/2)$ if $r \geq L/4$ (where the slope c'_1 is small, so that within *small* aggregates F_m is roughly constant). The confining magnetic potential in our experiments is, therefore, roughly parabolic for $r < L/4$ (Fig. 2): $V_{C,M}(r) = c_1 r^2$; $c_1 = c'_1/2$. The coefficient c_1 is a function of the position of the interface relative to the magnet, H , and of the magnetization of the magnet, M .

The pairwise repulsive interactions in CAA's are usually modeled as $1/r^n$ (especially the $1/r$ Coulombic interaction) [26,27] or $\ln(1/r)$ [36]. The potential characterizing the hydrodynamic repulsion in our system scales as r^{-2} [cf. Eq. (4)]. This function decays more steeply with r than does Coulombic repulsion. Given, however, the similarities of ordering in Wigner-type systems with $1/r^n$ potentials [37,38], we expect our aggregates to show morphologies similar to those predicted for classical atoms with $1/r$ repulsive interactions. In fact, our previous results [29] qualitatively reproduced those obtained theoretically by Bedanov and Peeters

[27] for parabolic external confinement and Coulombic interparticle repulsion. The empirical Hamiltonian \hat{H} for our system is given by

$$\hat{H} = \sum_i c_1(H, M) r^2 + \sum_{i < j} c_2^{ij}(\omega, a_i, a_j, \rho) |r_i - r_j|^{-2}, \quad (10)$$

in which c_1 and c_2^{ij} are constants that depend on parameters indicated in the parentheses, and the summation runs over all the disks composing an aggregate (“an atom”).

III. AGGREGATES OF SPINNING DISKS— EXPERIMENTAL RESULTS

A. Classical atoms

Most literature on classical artificial atoms focuses on the organization of *identical* particles. We realized the models of such generic CAA’s in previous work, in which we studied aggregates composed of disks of the same radii. The symmetrical, multishell structures we observed are described elsewhere [29], and will not be discussed here. We note that the morphologies of these patterns were in excellent agreement with the theoretical results obtained by others [26–28]. Here, we describe aggregates in which one disk (which, for the reasons discussed below, we will refer to as “a nucleus”) of diameter d_1 is larger than the other n small disks of diameter d_2 (“the electrons”); we denote these aggregates using the notation $[d_1, n d_2]$. From our theoretical analysis [Eq. (5)], we know that the hydrodynamic repulsion generated by the large disk is larger than the hydrodynamic force generated by any of the small disks. The theory does not tell us, however, the extent to which the presence of the big disk will affect the morphology of an aggregate, nor whether it will dictate the organization of the small disks.

The smaller disks used in the experiments were 1.27 mm in diameter and were doped with 15% by weight of magnetite. We examined systems in which bigger disks had diameters from 1.57 to 2.42 mm; the PDMS core of the larger disk had the same magnetic content as that of the smaller disks. Unless otherwise specified, the experiments were performed at $\omega = 400$ rpm and with $H = 3.5$ cm. When the size difference was small (OD of the big disk less than ~ 2 mm), the morphologies of the aggregates were highly dependent on initial conditions (i.e., initial position of the big disk with respect to other disks); for a given number of small disks we observed a plethora (\sim tens) of stable polymorphic patterns.

1. [2.08, n 1.27] “atoms”

When the diameter of the big disk was increased to 2.08 mm (Fig. 4), the situation changed drastically. The large disk reliably occupied the central position (on the axis of rotation of the magnet), and the remaining disks organized around it. This behavior was observed irrespective of the initial conditions: the big disk always ended in the center of the aggregate. In other words, the big disk constituted a “nucleus,” which organized the small disks around it (Fig. 4). For the

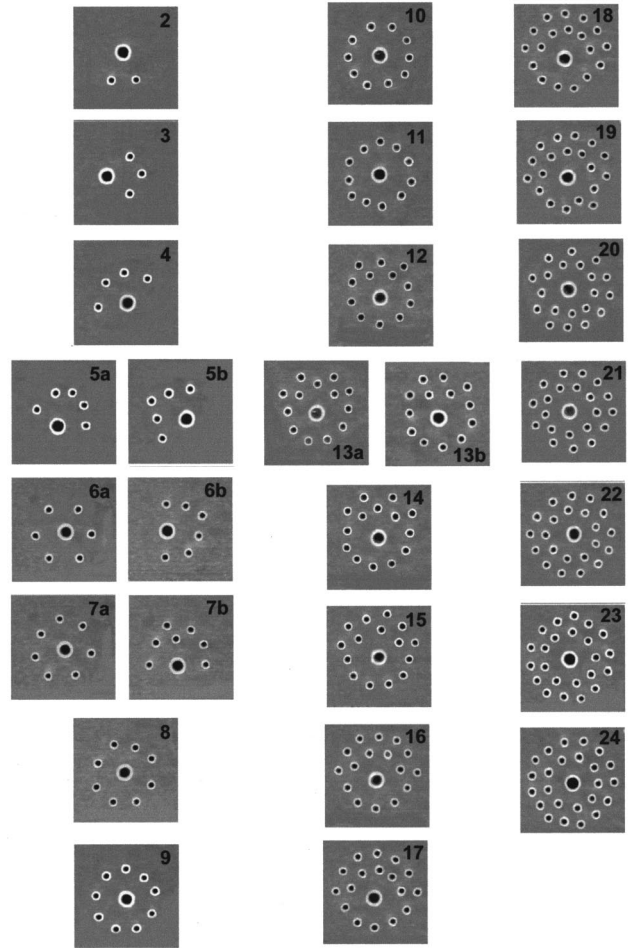


FIG. 4. Stable configurations for “atoms” composed of one large (2.08 mm in diameter) and several smaller (1.27 mm in diameter) disks. The numbers of smaller disks are indicated in the pictures. All aggregates were prepared at $\omega = 400$ rpm, on the EG-H₂O air interface 35 mm from the top face of the magnet.

number of small disks $n < 5$, the circular shells of “electrons” are incomplete, with the “electrons” orbiting around the “nucleus” in clusters.

We note that the asymmetry of these aggregates can be regarded as an example of emergent behavior [17]. An intriguing observation about these structures is that they apparently *do not* represent global energetic minima (the repulsive forces can be minimized by positioning the small disks at the vertices of a regular polygon around the large disk).

For $n = 6$ and $n = 7$, there are stable structures of two kinds: one, in which the small disks form closed shells (6a and 7a in Fig. 4) and a second, in which the shells are incomplete (6b and 7b). Both types of structures are stable, with the closed-shell aggregates occurring slightly more frequently ($\sim 60\%$ of the cases in 20 independent experiments). Eight and nine small disks ($n = 8$ and $n = 9$) form closed shells. For $n = 10$, two types of ordering are observed: a single shell with ten disks, and a double shell structure with nine disks in the inner shell and one in the outer shell. We therefore conclude that the first shell can accommodate not more than nine or ten small disks. It is interesting to compare

this observation with a qualitative theoretical prediction. If we construct an aggregate in which the large disk (2.08 mm) occupies the central position, and the small disks (1.27 mm) are on a circle around it, and if we stipulate the ratio of distances between the disks $[d(2.08 \text{ mm}-1.27 \text{ mm})/d(1.27 \text{ mm}-1.27 \text{ mm})]$ to be equal to that measured for pairs of disks [≈ 1.5 , Fig. 3(b)], then we can fit only approximately nine small disks onto a circle around the large disk.

For $n=11$ to $n=14$, we observed two-shelled aggregates, with eight electrons in the first shell and an incomplete second shell. The number of disks in the first shell is *lower* than for $n=9$ and $n=10$, and the disks in the outer shell tend to stay together (in a cluster), rather than be distributed equidistantly on the perimeter of the shell (reminiscent of structures 6b and 7b). Again, this type of behavior cannot be rationalized based on simple pairwise interactions in the system. We speculate that hydrodynamic effects caused by the precession of the entire aggregate play a role here: one possibility would be that the morphologies we observe reduce the hydrodynamic drag on a processing aggregate.

For $n=15$ to $n=19$ there are nine electrons in the first shell (except for 17a, where there are only eight), and the second shell is not closed. Notice that in most of these aggregates (apart from 15 and 17a) there is one electron trapped between the first and the second shells (cf. with structure 10b). This one electron is a center of a substructure (a pentagon in 16, a hexagon in 17b, 18, 19); in our previous work we observed that pentagons and hexagons are particularly stable morphologies for disks of equal size. The details of the ordering seem to be quite intricate: in addition to hydrodynamic effects associated with the precession of the entire aggregate, the existence of stable substructures might affect the morphology of the aggregates.

At $n=20$ the outer shell closes, and the number of disks in the first shell drops to seven or eight; this drop in population of the first shell might be thought of as a result of hydrodynamic repulsive forces exerted by the outer shell that squeezes (and shrinks) the inner shell. When additional disks are added to this structure, their number in the inner shell slowly increases to reach 9 at $n=24$; the occupancy of the outer shell also increases to reach 15 at $n=24$. The (9,15) configuration at $n=24$ is the last one in which two shells are observed in our experimental system. Interestingly, 15 is the maximum occupancy predicted for the outer shell based on the argument of polygonal packing and constant interdisk separations (cf. discussion of the occupancy of the first shell). For $n=25$, one electron is positioned in the third shell; this shell, however, experiences disruptive boundary effects due to inhomogeneities in the magnetic field near the edges of the magnet; thus, we do not describe aggregates with $n>24$.

2. [2.42, n 1.27] “atoms”

When the size of the nucleus is increased to 2.42 mm, the general trends in ordering of the aggregates are similar to those described for [2.08, n 1.27] atoms (Fig. 5). The first shell closes at $n=8$ and expands until $n=11$ (the maximum number of disks in the first shell estimated by the polygon

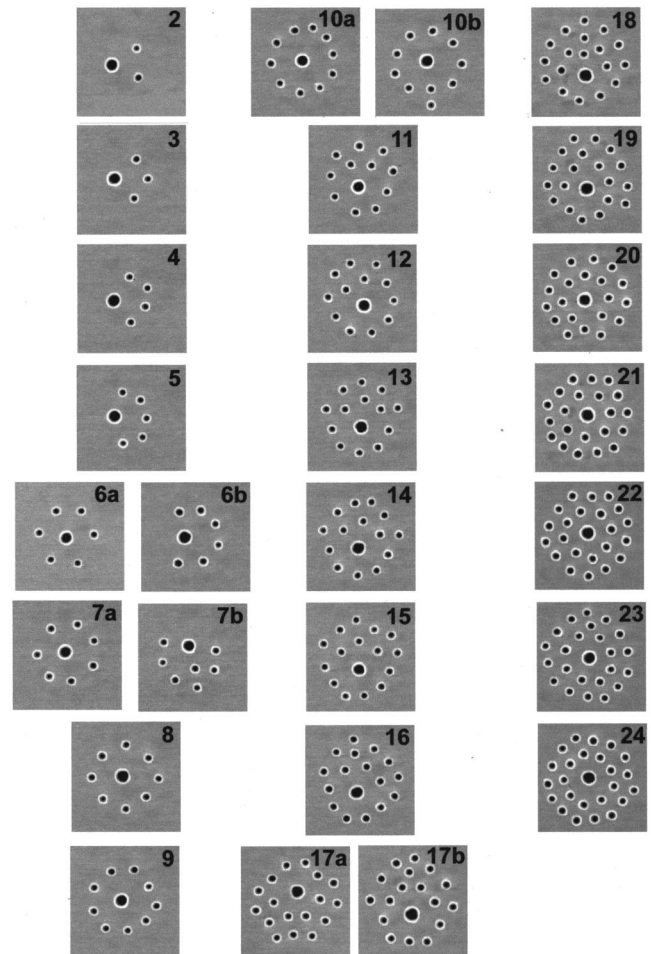


FIG. 5. Stable configurations for “atoms” composed of one large (2.42 mm in diameter) and several smaller (1.27 mm in diameter) disks. The numbers of smaller disks are indicated in the pictures. All aggregates were prepared at $\omega=400$ rpm at the EG-H₂O/air interface 35 mm from the top face of the magnet. The text discusses differences between the morphologies of these aggregates and those shown in Fig. 3 (where the large disk had a diameter of 2.08 mm).

method is 12). The double-shell structures that form for $n > 11$, usually have nine electrons in the first shell; the exceptions are atoms with $n=17-19$, which have ten electrons in the inner shell. We note that this increase in the occupancy of the first shell is observed just before the closing of the second shell ($n=20$). The morphologies of the observed structures are somewhat simpler than in the [2.08, n 1.27] system. In particular, we did not see any disks trapped between the two shells. We hypothesize that the morphology of an aggregate is governed predominantly by hydrodynamic repulsions involving the large nucleus; the substructures (pentagons and hexagons of small disks with one disk trapped between the shells) that influenced the shapes of some [2.08, n 1.27] atoms are apparently less frequent in [2.42, n 1.27] aggregates. The lower than expected occupancy of the first shell (9,10 instead of 12 expected on the basis of the “polygon” argument) might be the consequence of the competition between hydrodynamic repulsion and

confining magnetic forces. High repulsion from the large central disk tends to push the small disks further (than in [2.08, n 1.27] atoms) out, while the magnetic forces tend to draw them in; smaller shells give higher interdisk energy, but they allow removing the disks from the region of high magnetic energy (the periphery).

3. Dependence of atom morphology on rotational speed

Hydrodynamic repulsion between spinning pieces composing an aggregate increases with rotational speed. Therefore, the distances between the disks and, consequently, the sizes of the aggregates increase with ω . The effects associated with increasing (400→600→800 rpm) ω on the geometries of [2.42, n 1.27] atoms are summarized in Table I. For $n < 10$, atoms expand preserving the low-speed geometry and the ratio of interparticle distances. For $n = 11$, and for atoms with an open outer shell ($n = 12-19$), three types of rearrangements are possible: (i) a disk can be “promoted” to the outer shell ($n = 11, 18, 19$), (ii) an extra disk can be included in the inner shell ($n = 12, 13, 14, 16, 17$), or (iii) an atom can preserve its geometry ($n = 15$). For configurations with a closed outer shell, the morphology does not change when ω is increased.

4. Qualitative rules describing organization in artificial atoms

We conclude the description of atomlike aggregates by summarizing qualitative rules governing their structures. (1) The largest disk (a nucleus) occupies the central position on the axis of rotation of the magnet. (2) Smaller disks (electrons) organize into shells around the large disk. (3) The larger the size difference between the nucleus and electrons, the simpler the morphologies of the aggregates. (4) Shells are populated consecutively, i.e., the second shell fills, only after the first shell is completed. (5) When the size of an atom is not too large, the occupancies of the shells can be predicted by simple geometric considerations (polygon method). (6) Closed-shell structures are more stable than open-shell structures.

B. Classical artificial molecules

The practical importance of chemistry (and to a lesser degree, physics) lies in its ability to prepare (synthesize) large molecular aggregates from smaller components, and to provide rules governing chemical transformations. We sought to realize at least an ersatz version of such a “synthetic ability” in our macroscopic system by preparing structures that are more complex than our classical “atoms” and that resemble diatomic molecules. Specifically, we prepared aggregates of disks in which two disks are larger than the others. We investigated (i) a “homonuclear molecule” (2.42 mm large disks and 1.27 mm small disks) and (ii) a “heteronuclear molecule” in which one large disk is 2.42 mm in diameter and the other is 2.08 mm. We found that the organization of disks in these molecular aggregates is quite predictable and can be described by simple rules.

TABLE I. Summary of the observed morphologies of the [2.42, n 1.27] atoms at various rotational speeds. The notation x,y for two-shelled structures gives the numbers of small disks in the inner and the outer shells, respectively.

| n | 400 rpm | 600 rpm | 800 rpm |
|-----|--------------|---------|---------------|
| 1 | 1 | 1 | 1 |
| 2 | 2 | 2 | 2 |
| 3 | 3 | 3 | 3 |
| 4 | 4 | 4 | 4 |
| 5 | 5 | 5 | 5 |
| 6 | 6 | 6 | 6 |
| 7 | 7 | 7 | 7 |
| 8 | 8 | 8 | 8 |
| 9 | 9 | 9 | 9 |
| 10 | 10 | 10 | 10 |
| 11 | 11 | 10,1 | 10,1 |
| 12 | 9,3 | 10,2 | 10,2 |
| 13 | 9,4 | 9,4 | 10,3 |
| 14 | (9,5),(10,4) | 10,4 | (10,4),(11,3) |
| 15 | 9,6 | 9,6 | 9,6 |
| 16 | 9,7 | 10,6 | 10,6 |
| 17 | 10,7 | 10,7 | 9,8 |
| 18 | 10,8 | 10,8 | 9,9 |
| 19 | 10,9 | 10,9 | 9,10 |
| 20 | 9,11 | 9,11 | 9,11 |
| 21 | 9,12 | 9,12 | 9,12 |
| 22 | 9,13 | 9,13 | 9,13 |
| 23 | 9,14 | 9,14 | 9,14 |
| 24 | 9,15 | 9,15 | 9,15 |

1. Homonuclear [2.42, 2.42, n 1.27] molecules

Figure 6 gives the exhaustive list of structures of “diatomic molecules” with 2.42-mm nuclei and up to $n = 10$ of 1.27-mm electrons. For $n < 9$, the electrons organize into groups on either side of the axis joining the nuclei. All possible combinations are allowed, provided that the number of small disks in one group does not exceed seven. One can rationalize these structures by noting that (i) the small disks tend to occupy regions of closed circulation on both sides of the pair of nuclei (streamlines around a pair of spinning disks are discussed in [29]), and (ii) small disks are cleared from the regions near the axis joining the nuclei, where the velocity of the flow produced by an adjacent nucleus is high. The separation between the disks in each cluster is roughly constant and the clusters have at least mirror (or occasionally C_2) symmetry.

For $n = 9$ and $n = 10$, the clusters on two sides of the symmetry axis join to form an open shell. The structures observed are unique, i.e., we do not see polymorphs. The molecule with $n = 11$ is the last one with an open shell (Fig. 7), structures with $n > 11$ all have closed shells (one or more). Closed-shell structures for $11 < n < 26$ have many polymorphs (Fig. 7 shows the representative examples) that, however, are described by surprisingly simple rules: (1) The inner shell is always closed and has $n_1 = 10-13$ disks, n_1

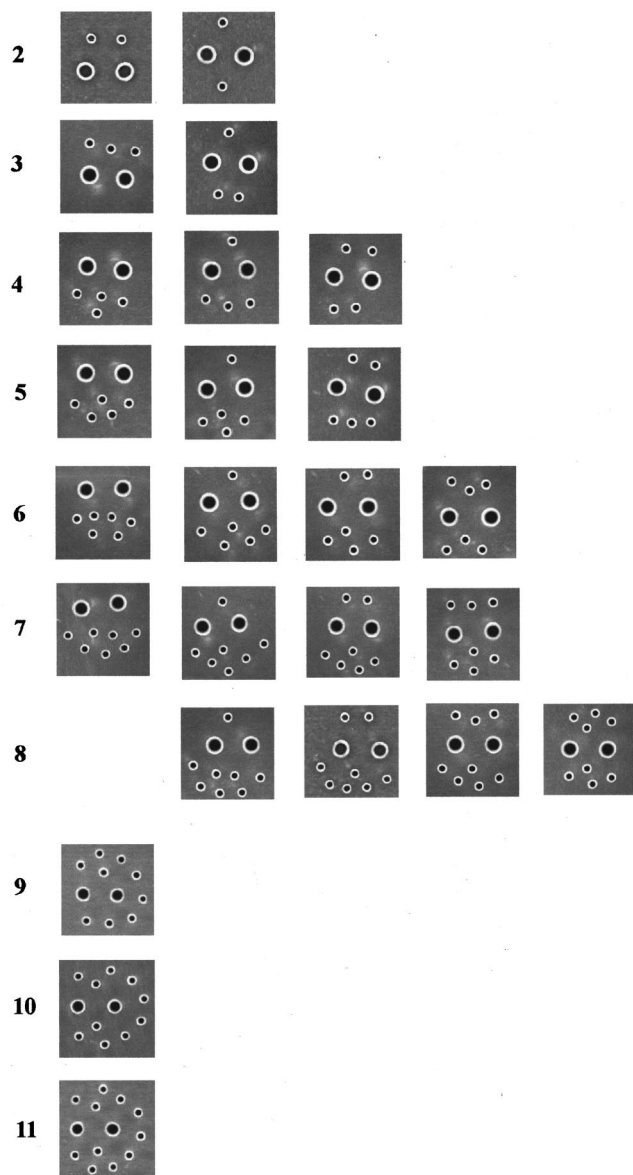


FIG. 6. Exhaustive list of stable configurations of aggregates (“homonuclear molecules”) composed of two large disks (OD 2.42 mm) and $n < 10$ smaller disks (1.27 mm in diameter). For $n < 9$, small disks organize into two groups (“clusters”) on the opposite sides of the axis joining the centers of the large disks; all possible combinations are allowed, provided that the number of disks in each group does not exceed seven. For $n = 9 - 11$, the two groups of disks meet on one end to give a hooflike structure.

increases steadily with n ; (2) The $n - n_1$ second-shell disks organize in clusters similar to those shown in Fig. 6; (3) The number of disks in each cluster does not exceed seven. The observed polymorphs all have an identical inner shell and differ only in the distribution of disks between the outer-shell clusters.

“Molecules” with $26 < n < 32$ are unstable. For these n 's, the disks in the outer shell are constantly sliding (“avalanching”) with respect to the inner shell; the clusters of second-shell disks are too large to be stable (< 8) but are also too small to connect to form a stable, closed second shell. The

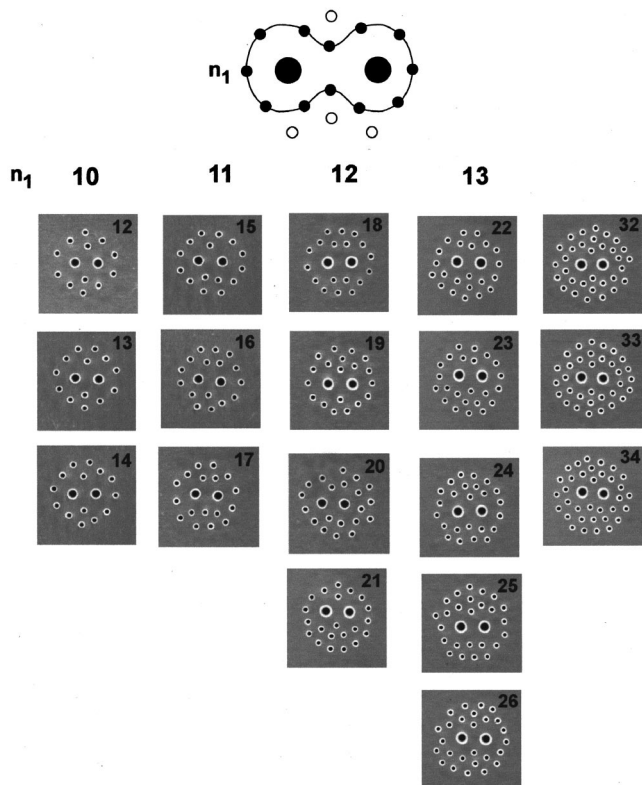


FIG. 7. Representative stable configurations of “homonuclear molecules” (two 2.42-mm “nuclei” and $n > 10$ 1.27-mm “electrons”). The small disks organize into shells around the “nuclei.” The first shell (defined in the schematic diagram) can accommodate n_1 “electrons”; n_1 increases monotonically with n . The second-shell “electrons” organize according to rules similar to those shown in Fig. 5—therefore, for a given n , there are several ways of organizing the second-shell disks. The occupancy n_1 of the first shell, however, is unique for a given n . For $n = 27 - 31$, no stable structures were observed as the disks in the second shell were constantly sliding with respect to the first shell. All aggregates in this figure were prepared at $\omega = 400$ rpm at the EG-H₂O/air interface 35 mm from the top face of the magnet.

second shell closes only at $n = 32$ to give a highly symmetric aggregate. Stable, symmetric aggregates are also seen for $n = 33$ and $n = 34$. For $n = 35$, one disk is placed in the third shell. Because the third-shell disks experience inhomogeneous magnetic fields that reduce the stabilities of the aggregates, they are not discussed here. We emphasize that these instabilities seem to be a characteristic of the experimental system, not a fundamental instability of large numbers of disks.

2. Heteronuclear [2.42, 2.08, n 1.27] molecules

Figure 8 shows representative structures of “heteronuclear molecules.” These structures correspond to two different experiments: in the column on the right, we show aggregates formed at $H = 35$ mm while in the column at the left, we show aggregates formed at $H = 30$ mm (if the structures are the same at both values of H , only one column is shown). The aggregates that form when the interface is more

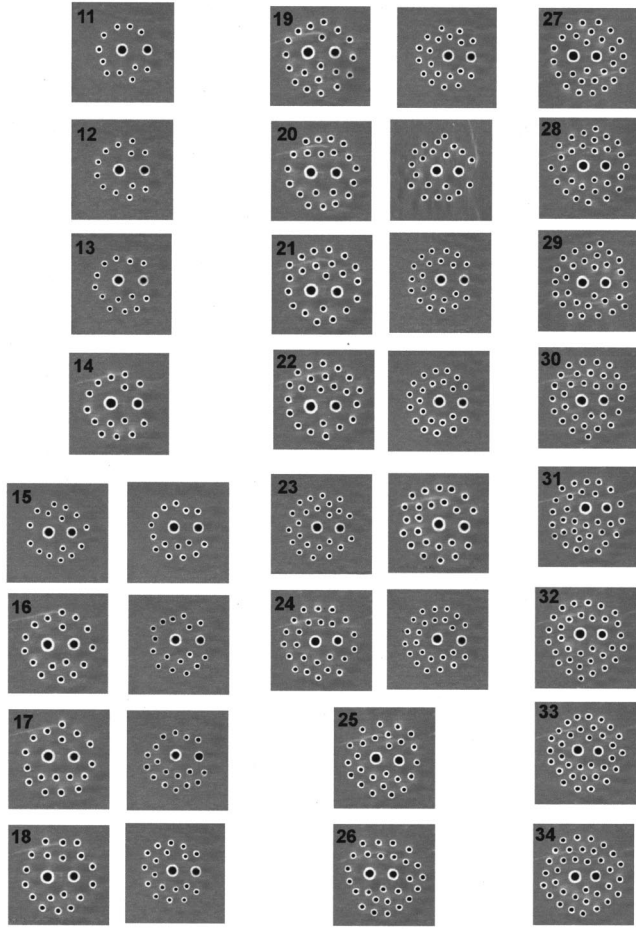


FIG. 8. Representative configurations of “heteroatomic” (two large disks of diameters 2.42 and 2.08 mm) aggregates at two different values of H (35 mm, left column and 30 mm, right column). If the structure at $H = 35$ mm differed from that at $H = 30$ mm, both morphologies are shown. At $H = 35$ mm and for $n < 15$, only the open-shell structures were observed. For $n \geq 15$, all the aggregates had closed shells with the occupancy of the first shell $n_1 \sim 12$. At $H = 30$ mm, open-shell structures were seen for $n < 25$; closed-shell structures formed above $n = 25$. All experiments were done at $\omega = 400$ rpm with disks spinning at an EG-H₂O/water interface.

distant from the magnet ($H = 35$ mm) are qualitatively similar to the homonuclear molecules. For $n < 15$, only open-shell structures are observed; for $n > 15$ the inner shell is closed and outer shells are being populated. All structures up to $n = 34$ are stable (unlike in “homonuclear” aggregates). The inner shell can adopt 10–12 disks (a full list of configurations is given in Table II).

When H is decreased to 30 mm, the morphologies and dynamic properties of aggregates with $n < 25$ change. Open-shell structures are observed and the smaller nucleus starts precessing around the larger one (at $H = 35$ mm the nuclei precessed around their center of mass). This behavior is partly explained by the effect of higher magnetic field at smaller H : the nuclei, in addition to spinning around their axes, start translating under the influence of the rotating field (they “follow” the magnet). Since the hydrodynamic drag on the smaller nucleus is less than on the larger one, it is the

TABLE II. Configurations of heteronuclear [2.42, 2.08, n 1.27] “molecules” observed for two locations of the interface ($H = 35$ mm, and $H = 30$ mm). The notation x, y gives the numbers of small disks in the inner and in the outer shells, respectively. The asterisk indicates that the configurations at both values of H are identical. We indicate by “~” the cases, where the assignment of disks to inner and outer shells is not obvious.

| n | $H = 35$ mm | $H = 30$ mm | n | $H = 35$ mm | $H = 30$ mm |
|-----|-------------|-------------|-----|-------------|-------------|
| 11 | 10,1 | 10,1* | 23 | 12,11 | 11,12 |
| 12 | 10,2 | 10,2* | 24 | 12,12 | 12,12 |
| 13 | 10,3 | 10,3* | 25 | 12,13 | 12,13* |
| 14 | 10,4 | 10,4* | 26 | 12,14 | 12,14* |
| 15 | 11,4 | 11,4 | 27 | 12,15 | 12,15* |
| 16 | 11,5 | 11,5 | 28 | ~12,16 | ~12,16* |
| 17 | 12,5 | 11,6 | 29 | ~12,17 | ~12,17* |
| 18 | 12,6 | 8,10 | 30 | ~12,18 | ~12,18* |
| 19 | ~12,7 | 10,9 | 31 | ~12,19 | ~12,19* |
| 20 | ~12,8 | ~10,10 | 32 | ~12,20 | ~12,20* |
| 21 | 12,9 | 10,11 | 33 | 12,21 | 12,21* |
| 22 | 12,10 | 11,11 | 34 | 12,22 | 12,22* |

2.08-mm disk that starts precessing. Interestingly, when the second-shell closes ($n \sim 25$ and higher), the aggregates formed at $H = 30$ mm and $H = 35$ mm are indistinguishable; we presently do not have a convincing explanation for this similarity.

3. Possible extensions

The last experiment illustrates amply the complexity of our system: slight adjustments in either hydrodynamic and magnetic properties of the spinners can result in totally new types of organization and behavior. We close our discussion, with an example of how new characteristics can be introduced into our aggregates by changing the magnetic content of the disks (Fig. 9). The structure shown on the lower right is composed of disks of equal sizes, yet the spacing between the shells is different than that between the disks. Moreover, the inner shell rotates with respect to the outer shell. How much more complex structures can be achieved by *varying several parameters simultaneously* is to be established.

CONCLUSIONS

The self-assembly of spinning disks into macroscopic artificial “atoms” and “molecules” is the consequence of the interplay between attractive (paraboliclike external confining potential) and repulsive ($1/r^3$ pairwise repulsion) interactions. Since qualitatively similar interactions govern the physics of microscopic systems of classically behaving particles, we propose that our experimental system might be used to model, at least approximately, certain microscopic assemblies. For instance, the aggregates of spinning disks, in which the hydrodynamic repulsive forces scale as $1/r^3$, might be used to mimic microsystems with charge-dipole-type interactions. The hydrodynamic repulsions can be tuned to obey other scaling laws by changing their shapes (e.g.,

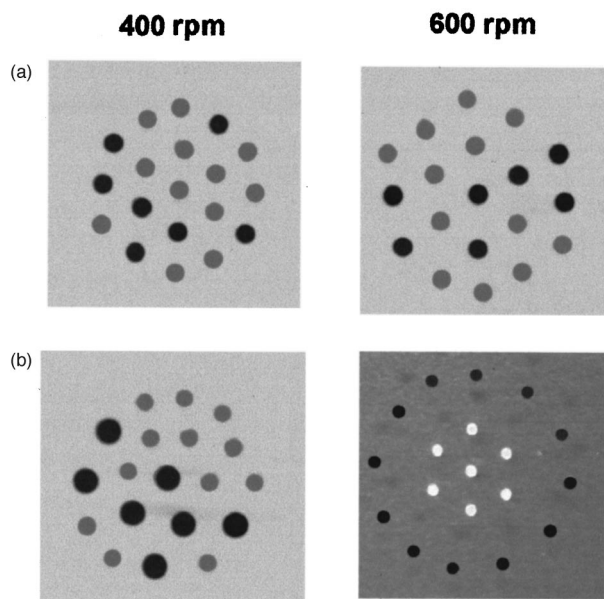


FIG. 9. Pictures in (a) and (b) show the aggregates formed by disks of different magnetic loading. In (a), the difference in loading (gray disks, 10% magnetite; black disks, 15%) is too small to alter the morphology of the pattern: no segregation of particles is seen at 400 rpm or 600 rpm. In (b), in the picture on the left, the disks differ in both the magnetite content and in size (gray, 1.27 mm; black, 1.57 mm) yet they do not segregate. Segregation is observed when the difference in magnetic loading is increased: in the picture on the right, the central nucleus (white disks) is formed by 1.27-mm disks doped with 30% magnetite, while the outer layer (black disks) has 1.27-mm disks of magnetite content of 15%. The central nucleus precesses faster than the outer shell—as a consequence, this nucleus exerts an additional hydrodynamic repulsion on the outer shell and the interlayer spacing is larger than in (a) at the same ω .

two spinning rectangles repel differently than two spinning disks); we are presently quantifying interaction profiles for spinning objects of different shapes. Different profiles of the confining magnetic potentials can also be prepared. Because of the flexibility of design, simplicity of the experimental setup, and the robustness of the results, our system can be a useful tool complementing other experimental and computational techniques used to investigate the organization of microscopic classical particles.

We also believe that our work can have implications in three other areas.

(i) In hydrodynamics, the spinning disks (or objects of other shapes) can help study the interactions between vortices [39,40] or vortex patches [41]. The theoretical description and controlled experimental realization of vortex-vortex interactions are sometimes prohibitively complicated—the experimental simplicity of our system might offer a remedy to these problems.

(ii) In self-assembly and materials science, the systems of spinning objects can serve as precursors for open lattices to be used in photonic bandgap materials or molecular sieves. The potential of our system in this application would, however, only be realized if the sizes of the objects were made two or three orders of magnitude smaller than they presently are; we are currently working on systems of spinners of sizes $\sim 100 \mu\text{m}$.

(iii) Structures of some of our aggregates indicate collective/emergent behavior; systems having such characteristics are of potential relevance to the subject of complexity [16,17]. The ease of preparation of many complex structures is a remarkable feature of this system. For instance, the aggregates of spinning disks are one of the simplest rationally designed systems in which symmetry breaking can be observed.

The analogy we imply by the phrases “classical artificial atoms,” and by the use of terms “nucleus” and “electrons” to describe components of the systems, is more nomenclatural than physical. Clearly, the mutually repulsive particles cannot mimic atomic and subatomic assemblies in which opposite charges are present. The size of the spinning object might correspond to the magnitude of electric charge, but there is no counterpart of the *sign* of the charge. Making systems of spinners of different “signs,” with both attractive and repulsive interactions remains a problem we are trying to solve. These systems do, however, have very primitive analogies to atoms at the level of central potentials and particle-particle repulsion.

ACKNOWLEDGMENTS

This work has been supported by the DOE (Contract No. 00ER45852); H.A.S. thanks the Harvard MRSEC for financial support.

-
- [1] J. K. Whitesell, *Organized Molecular Assemblies in the Solid State* (Wiley, New York, 1999).
- [2] D. Philp and D. J. F. Stoddart, *Angew. Chem. Int. Ed. Engl.* **35**, 1155 (1996).
- [3] O. V. Lounasmaa and E. Thuneberg, *Proc. Natl. Acad. Sci. U.S.A.* **96**, 7760 (1999); **96**, 26 (1999); D. A. Schechter, D. H. E. Dubin, K. S. Fine, and C. F. Driscoll, *Phys. Fluids* **11**, 905 (1999).
- [4] M. M. Burns, J. M. Fournier, and J. A. Golovchenko, *Science* **249**, 749 (1990).
- [5] T. Shinbrot, *Nature (London)* **389**, 574 (1997).
- [6] N. Bowden, S. Brittain, A. G. Evans, J. W. Hutchinson, and G. M. Whitesides, *Nature (London)* **393**, 146 (1998).
- [7] N. Bowden, I. S. Choi, B. A. Grzybowski, and G. M. Whitesides, *J. Am. Chem. Soc.* **121**, 5373 (1999).
- [8] C. A. Murray and D. G. Grier, *Am. Sci.* **83**, 238 (1995).
- [9] M. Gomez Lopez, J. A. Preece, and J. F. Stoddart, *Nanotechnology* **7**, 183 (1996).
- [10] D. A. Thompson, *On Growth and Form* (Dover, New York, 1992).
- [11] J. A. Shapiro, *Annu. Rev. Microbiol.* **52**, 81 (1998).
- [12] H. Berg and H. E. Budrene, *Nature (London)* **376**, 49 (1995).

- [13] A. Koschmider, *Benard Cells and Taylor Vortices* (Cambridge University Press, Cambridge, 1993).
- [14] S. Jakubith, H. H. Rotermund, W. Engel, A. von Oertzen, and G. Ertl, *Phys. Rev. Lett.* **65**, 3013 (1990).
- [15] Y. Engelborghs, *Biosens. Bioelectron.* **9**, 685 (1994).
- [16] K. Lindgren, C. Moore, and M. Nordahl, *J. Stat. Phys.* **91**, 909 (1998).
- [17] R. Singh, V. M. Maru, and P. S. Moharir, *J. Nonlinear Sci.* **8**, 235 (1998).
- [18] J. J. Thomson, *Philos. Mag.* **7**, 237 (1904); B. Partoens and F. M. Peeters, *J. Phys.: Condens. Matter* **9**, 5383 (1997).
- [19] A. M. Mayer, *Nature (London)* **18**, 258 (1878).
- [20] C. E. Wieman, D. E. Pritchard, and D. J. Wineland, *Rev. Mod. Phys.* **71**, S253 (1999).
- [21] W. M. Itano, J. C. Bergquist, J. J. Bollinger, and D. J. Wineland, *Phys. Scr., T* **59**, 106 (1995).
- [22] R. Schruch, *Phys. Scr., T* **59**, 77 (1995).
- [23] U. Albrecht and P. Leiderer, *Can. J. Phys.* **65**, 1536 (1987).
- [24] R. Bubeck, C. Bechinger, S. Naser, and P. Leiderer, *Phys. Rev. Lett.* **82**, 3364 (1999).
- [25] T. Ogino, H. Hibino, and Y. Homma, *Crit. Rev. Solid State Mater. Sci.* **24**, 227 (1999); R. Rinaldi, *Int. J. Mod. Phys. B* **12**, 471 (1998).
- [26] Y. E. Lozovik and V. A. Mandelshtam, *Phys. Lett. A* **145**, 269 (1990); **165**, 469 (1992).
- [27] V. Bedanov and F. M. Peeters, *Phys. Rev. B* **51**, 7700 (1995); **49**, 2667 (1994).
- [28] F. Bolton and U. Rössler, *Superlattices Microstruct.* **13**, 139 (1993).
- [29] B. A. Grzybowski, H. A. Stone, and G. M. Whitesides, *Nature (London)* **405**, 1033 (2000).
- [30] We verified experimentally that two spinning magnetically doped spheres placed either at a liquid-air or liquid-liquid interface repel each other via a hydrodynamic repulsion qualitatively similar to that between two spinning disks. In our experiments, we used disks rather than spheres because of the difficulties associated with fabrication of uniform, magnetically doped polymeric spheres ~ 1 mm in diameter.
- [31] Rubinow and Keller considered the translation \vec{V}^* (due to an applied force) and rotation (due to an applied torque) of a sphere at small but finite Reynold's numbers, and observed that there is a lift force \vec{F}_L (i.e., a force perpendicular to the direction of translation) of $\vec{F}_L = \rho a^3 \vec{V}^* \times \vec{\omega}$. Note that the predicted direction of this force is opposite to the direction we observe (and predict) for our system. This difference stems from the fact that in our system the sphere translates *with* the flow, rather than *relative to* it, as in Rubinow's calculation.
- [32] J. A. Schonberg and E. J. Hinch, *J. Fluid Mech.* **203**, 517 (1989).
- [33] T. R. Auton, *J. Fluid Mech.* **183**, 199 (1987).
- [34] E. M. Purcell, *Electricity and Magnetism* (McGraw-Hill, New York, 1985), Vol. 2, Chap. 11.
- [35] The magnetic dipole m of a disk (and thus, the magnetic force F_m) is proportional to the content of the magnetic material. Thus, in general, $F_m = O(ma^3)$.
- [36] R. Calinon, P. Choquard, E. Jamin, and M. Navet, in *Ordering in Two Dimensions*, edited by S. K. Sinha (Elsevier, New York, 1980), p. 317.
- [37] R. C. Gann, S. Chakravarty, and G. V. Chester, *Phys. Rev. B* **20**, 326 (1979).
- [38] J. Q. Broughton, G. H. Gilmer, and J. D. Weeks, *Phys. Rev. B* **25**, 4651 (1982).
- [39] T. H. Havelock, *Philos. Mag.* **11**, 617 (1931).
- [40] H. Aref and D. L. Vainchtein, *Nature (London)* **392**, 769 (1998).
- [41] D. G. Dritschel, *J. Fluid Mech.* **157**, 95 (1985).